Am J Transl Res 2015;7(2):348-355
www.ajtr.org /ISSN:1943-8141/AJTR0003201

Original Article

Combined micro CT and histopathology for evaluation of skeletal metastasis in live animals

Christopher P Geffre[1], Erika Pond[2], Gerald D Pond[3], Isis C Sroka[4], Jaime M Gard[2], Bethany A Skovan[2], William E Meek[2], Terry H Landowski[5], Raymond B Nagle[1], Anne E Cress[2,6]

[1]Department of Pathology, University of Arizona College of Medicine, Tucson, AZ 85724, USA; [2]University of Arizona Cancer Center, Tucson, AZ 85724, USA; [3]Department of Medical Imaging, University of Arizona College of Medicine, Tucson, AZ 85724, USA; [4]Department of Pharmacology, University of Arizona College of Medicine, Tucson, AZ 85724, USA; [5]Department of Medicine, University of Arizona College of Medicine, Tucson, AZ 85724, USA; [6]Department of Cellular and Molecular Medicine, University of Arizona College of Medicine, Tucson, AZ 85724, USA

Received October 17, 2014; Accepted January 5, 2015; Epub February 15, 2015; Published February 28, 2015

Abstract: Bone is a favored site for solid tumor metastasis, especially among patients with breast, lung or prostate carcinomas. Micro CT is a powerful and inexpensive tool that can be used to investigate tumor progression in xenograft models of human disease. Many previous studies have relied on terminal analysis of harvested bones to document metastatic tumor activity. The current protocol uses live animals and combines sequential micro CT evaluation of lesion development with matched histopathology at the end of the study. The approach allows for both rapid detection and evaluation of bone lesion progression in live animals. Bone resident tumors are established either by direct (intraosseous) or arterial (intracardiac) injection, and lesion development is evaluated for up to eight weeks. This protocol provides a clinically relevant method for investigating bone metastasis progression and the development of osteotropic therapeutic strategies for the treatment of bone metastases.

Keywords: Bone, metastasis, xenograft, prostate cancer, histopathology, micro CT

Introduction

Xenograft models of bone metastasis are powerful tools that can be used to examine the interactions of human tumor cells within the bone microenvironment [1]. Breast and prostate cancers are known to disseminate to bone and remain dormant [2, 3]. Loss of dormancy may be an explanation for known recurrence of these cancers, long after elimination of primary disease. Development of xenograft models with the ability to longitudinally analyze the progression of metastatic bone lesions can be useful for identification of metastasis promoter or suppressor genes, along with factors related to conversion of micro-metastatic lesions to clinically significant lesions. This combination protocol was developed to investigate lesion progression using micro-computed tomography (micro CT) and matched histopathology. Two different injection routes were also compared; both have been used with success by our group and others [4-8].

Many studies using small animal bone metastasis models have relied on Faxitron radiographic images to detect disease progression [9-11]. Faxitron analysis is rapid and inexpensive, but has limited resolution and cannot produce three-dimensional, quantifiable images of tumor induced bone loss. Micro CT is a cost effective x-ray based imaging method that provides high resolution (< 50 microns) three-dimensional images of bone [12], which is particularly relevant for highlighting cancer induced changes in bone. Matching micro CT images to corresponding histopathology sections can be technically challenging. The provided protocol details procedures for optimal micro CT scanning, image collection and analysis, intraosseous and intracardiac injection, harvesting, fixation, embedding and sectioning for optimal histopathology.

Materials and methods

Animals

Severe combined immunodeficiency (SCID) male mice were obtained through the Experimental Mouse Shared Services at the University of Arizona Cancer Center. All experimental procedures were performed with protocol approval of the University of Arizona's Institutional Animal Care and Use Committee (IACUC). Twelve Male SCID mice were at least 8-weeks old and screened at the beginning and end of the study via ELISA to ensure that circulating levels of IgG are less than 20 micrograms/ml (data not shown).

Cell line and culture conditions

The PC3-B1 cells are a subpopulation of the PC3 human prostate cancer cell line selected for their prominent bone homing phenotype and ability to produce progressive bone lesions in SCID mice as previously described [8, 13]. Cells were maintained at 37°C in a humidified atmosphere of 95% air and 5% CO_2 with Iscove's Modified Dulbecco Media (IMDM) (Mediatech Inc., cat. no. 10-016-CV) supplemented with 10% fetal bovine serum (PAA Laboratories Inc., cat. no. A15-201). Cells were screened for mycoplasma prior to use and cell line identity was verified using twelve different genomic markers for DNA fingerprinting using tetranucleotide motifs (STR profiles) (data not shown). Genomic verification was critical, as the identity of cell lines after passages in laboratories has been found to be problematic [14]. Cells were harvested with Dulbecco's phosphate buffered saline (D-PBS) containing 5 mM EDTA, centrifuged at 500 g for 3 minutes and resuspended in sterile D-PBS at $2x10^7$ cells/ml for intraosseous injections or $5x10^6$ cells/ml for intracardiac injections.

Intraosseous injection

Mice were anesthetized with isoflurane (Phoenix Pharmaceutical Inc., cat. no. 0010100), with an initial induction of 4%, maintained at 1.5-2% and delivered through a nose cone with a 1 L/min flow rate. Both knee joints were shaved and approximately $1.0x10^5$ PC3 cells in 5 µL of DMEM were injected using a 100 µl Hamilton type syringe with a 27 gauge needle. The needle was inserted into the intra condylar notch of the femur using a spinning motion. Cells were injected into the medullary space (approximately 0.3 cm proximal to the epiphyseal plate), with no suturing required. Ease in advancement of the needle indicated successful penetration of the medullary space. Unsuccessful insertion of the needle caused soft tissue surrounding the knee to expand upon cell injection. To control for surgical effects, 5 µL of DMEM was injected into the contralateral limb using the same technique. Following injection, 0.1 mg/kg buprenorphine (Western Medical, cat. no. 7292) was injected subcutaneously to minimize post procedure pain and animals were returned to cages for recovery.

Intracardiac injection

Mice were anesthetized with isoflurane (induction with 4%, maintained at 1.5-2% delivered through a nose cone, 1 L/min flow rate) and approximately $0.5x10^6$ cells in 0.1 ml of sterile D-PBS were injected using a 1 ml tuberculin type syringe with a 27 gauge needle. Mice were placed dorsally on the table with the needle inserted at the level of the elbow, between the 3rd and 4th or 4th and 5th intercostal space. Care was taken to remain on the left side of the animal's chest to ensure injection into the left ventricle. The presence of bright red arterial blood indicated a properly placed needle. If the left ventricle was not penetrated after three attempts, the mouse was excluded from the study. Following injection, 0.1 mg/kg buprenorphine was injected subcutaneously to minimize post procedure pain and animals were returned to cages for recovery.

Animal follow-up care

Following recovery from anesthesia all mice were observed briefly. Incorrectly placed intracardiac injections were indicated by early death, odd behavior or presence of chest tumor at necropsy. For intraosseous injections, animals were scanned by micro CT one day post injection to identify failed injections, indicated by needle tracks outside of the bone, soft tissue calcification or extrinsic cortical scalloping (data not shown). Twice weekly, animals were observed for critical signs of morbidity and weight was recorded. Animals were euthanized and removed from the study if any signs of pain or suffering were indicated, including: rapid, slow, shallow, or labored breathing, anorexia, cachexia, rapid weight loss, hunched posture, hypo- or hyperthermia, constipation, diarrhea,

Table 1. Micro CT detection of bone metastases following intra cardiac injection

Mouse	Week 3	Week 4	Week 5	Week 6	Week 7
1	RDF	RDFp	RDFp	***	***
	RPT	RPTp	RPTp		
	LDF	LDFp	LDFp		
	LF	LFp	LFp		
			***		
2	RPT	RPT	RPTp	RPTp	RPTp
	LDF	LDF	LDFp	LDFp	LDFp
	LPT	LPT	LPTp	LPTp	LPTp
			Pen	Penp	Penp
					***
3	RDF	RDF	RDFp	***	***
	RPF	RPF	RPFp		
	S3	S3	S3p		
			***		
4	RDF	RDFp	***	***	***
	RPT	RPTp			
	LDF	LDFp			
	LPT	LPTp			
		***			
5	RDF	RDF	***	***	***
	LDF	LDFp			
	LPT	LPT			
		***			
6	RIC	RIC	***	***	***
	RPT	RPT			
	LPT	LPT			
		***			
7	RPT	RPT	***	***	***
		RIC			
		LPT			
8	LIC	LIC	LIC	***	***
9	LDF	LDF	***	***	***
		LIC			

LDF, left distal femur; LF, left fibula; LIC, left iliac crest; LPT, left proximal tibia; Pen, os penis; RDF, right distal femur; RIC, right iliac crest; RPF, right proximal femur; RPT, right proximal tibia; S3, sacral vertebra 3; lower-case 'p' is a progressive lesion; *** mouse was euthanized.

impaired ambulation, lethargy, paralysis, nasal or ocular discharge, or imminent pathologic fractures indicated on micro CT as interpreted by the radiologist.

Micro CT equipment setup

Progressive lesions were evaluated using Siemens Inveon Micro CT Scanner and Inveon Research Workplace Software (IRW). Scans were limited to the abdomen and hind limb region to optimize resolution and minimize radiation exposure time. No correction was used for respiration and motion. Images were acquired at high resolution (Bin-4) with medium high magnification with conversion to Hounsfield Units (HU). The scanning protocol required 440 exposures over 220° with 375 milliseconds per projection with a 0.5 mm filter (filter wheel setting #2), 80 kV, 500 microA, and effective pixel width of 57 μm. Cobra software (Exxim, Pleasanton CA) was used to reconstruct images with downsampling of 1 and beam hardening correction. The Inveon Multimodality Imaging System (Siemens AG, Munich, Germany) utilized a standard CT camera with a high resolution, 12-bit x-ray imaging detector with 2048x3072 pixels configured for mouse imaging. The useable field was 8.4 cmx5.5 cm and the bed pallet was 38 mm. An isoflurane anesthetic portable vaporizer system (e.g. VetEquip Inc., Model. no. IT3) was utilized with a gas scavenging system (charcoal filtration) to prevent adverse health effects (e.g. central nervous system damage) to the mouse. The CT Real-Time Reconstruction System involved a high speed modified Feldkamp cone beam reconstruction algorithm to provide reconstructed image volumes within seconds of scan completion.

Micro CT scanning and collection of optimal images

Micro CT scans began at 1 week post-intraosseous injection and 3 weeks post-intracardiac tumor cell injection. All calibrations (e.g. center-offset, light/dark calibration) were done prior to scanning test animals. Animals were placed in the prone position on the CT mouse bed, with the tail towards the inside of the CT machine and anesthesia delivered via nose cone (2% isoflurane at 1 L/min flow rate). The hind legs were stretched symmetrically behind the mouse with flexed ankles gently anchored with tape. Consistent placement of animals was critical for accurate orientation and interpretation of sequential scans and scout images were obtained to establish scan parameters. After scanning, animals were injected subcutaneously with 1 ml sterile saline to aid in recovery from the anesthetic. Animals recovered for at

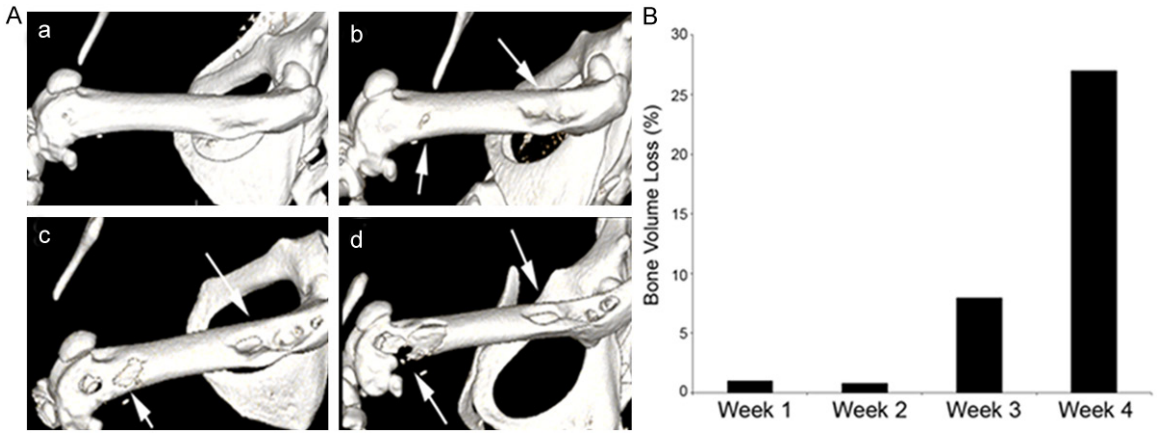

Figure 1. Micro CT analysis of progressive bone loss in a mouse femur directly injected with PC3-B1 prostate cancer cells. A. 3D micro CT analysis was performed at 1 week (a), 2 weeks (b) and 3 weeks (c) and 4 weeks (d) after direct tumor cell injection. Arrows demarcate tumor induced bone loss detected by 3D micro CT images. B. Quantification of total bone loss in the mouse femur was determined using 3D image analysis and IRW software (Siemens). Progressive femoral lesions in the same mouse demonstrated an 8% and 27% increase in bone volume loss by 3 and 4 weeks, respectively.

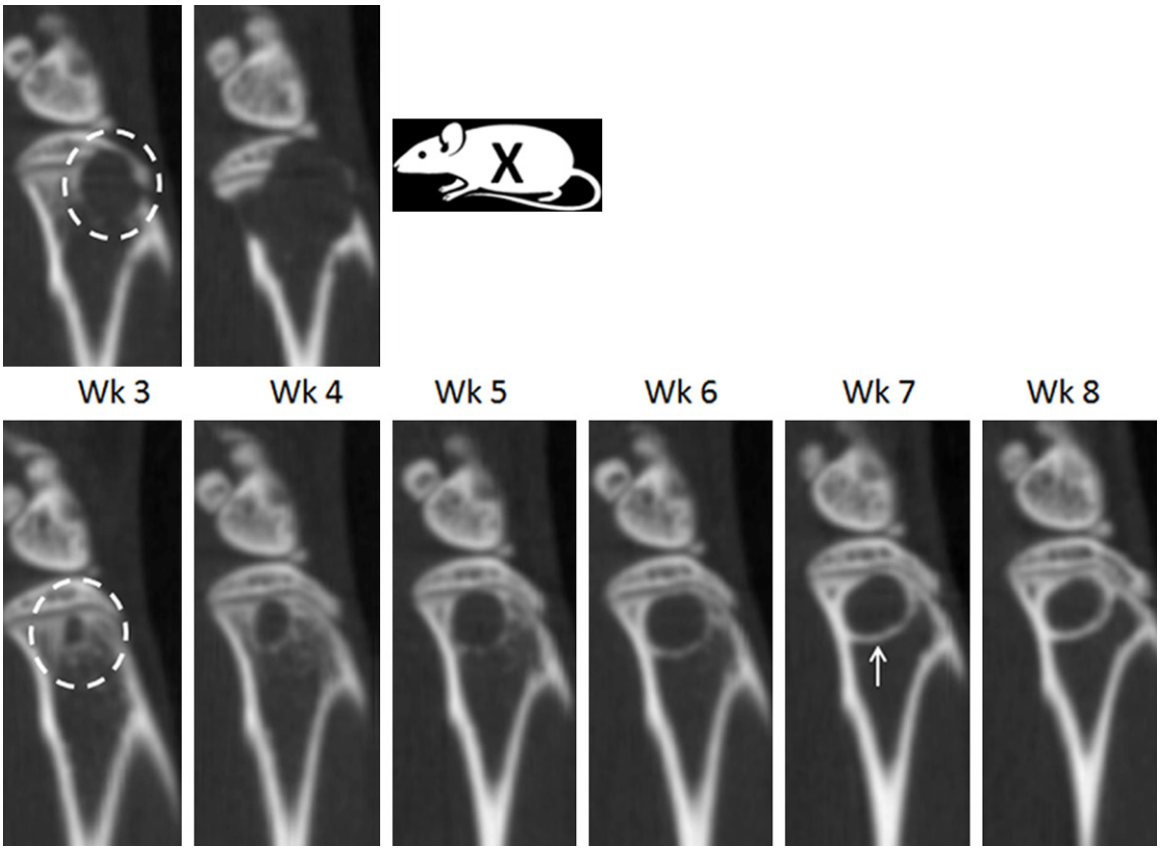

Figure 2. Micro CT analysis of progressive bone lesion in mouse femur following intracardiac injection. Identical sagittal sections from the same mouse containing a progressive bone lesion from week 3 to week 4 (top panel, Wk3-Wk4) and week 3 to week 8 (bottom panel, Wk3-Wk8). Aggressive lytic lesions appeared within the majority of animals by week 3 (top panel, Wk3, white circle) and breached the cortical bone by week 4 (top panel, Wk4), resulting in removal from the study (top panel, Wk5, X). In a minority of animals, a circular type lytic lesion increased from week 3 to week 6 (bottom panel, Wk3-Wk6). New bone growth (bottom panel, Wk7, white arrow) was first observed prominently at week 6, followed by cessation of lesion progression during week 6 to week 8.

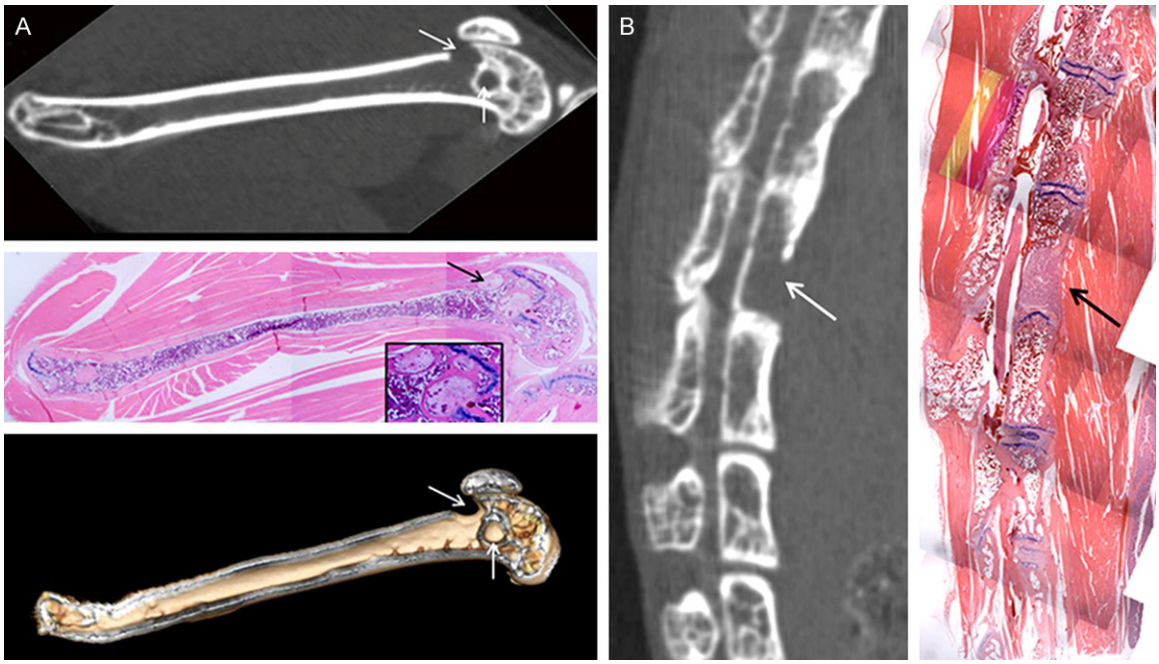

Figure 3. Precise micro CT and histological correlation of metastatic bone lesions. (A) Sagittal image of two femoral lesions (arrows) post intracardiac injection (A, top panel), histology of the same lesions (A, middle panel and inset) and 3D reconstructed image using the Siemens software (A, bottom panel). Another lesion near the patella breached the bone and another distinct lesion is present in the medullary space (B) Sagittal micro CT image of vertebral metastasis (B, left panel, white arrow) and corresponding histological section show tumor within one vertebral body (B, right panel, black arrow). The intervertebral discs are distinct (B, left panel, blue parallel stain).

least one hour before returning to the animal care facility. Each CT scan was completed in approximately 10 minutes and produced approximately 400 mGy of radiation, which is below the level known to alter tumor cell growth in vivo [15].

Micro CT image interpretation and analysis using IRW software

Micro CT images were reviewed weekly by a radiologist without knowledge of the treatment groups. Lesions were only recorded if observed in all three image views (axial, coronal, and sagittal). Once pathological lesions were confirmed, the location was recorded (**Table 1**). A lesion was identified as progressive if it increased in size or if a pathologic fracture was identified. Once the lesions of interest were identified, bone volume changes were tracked (**Figures 1**-**4**) using the IRW software. The bone containing the lesion of interest was selected and the bone volume was calculated. While specific commands for bone volume quantitation can vary by platform, utilization of the histogram and 'Magic Wand' tools were found to be the most useful with the Siemens IRW software.

Tissue harvest, processing and slide preparation for histopathology

At the end of the study, animals were euthanized via inhaled CO_2. Skin was removed from the hind limb and caudal portion of the mouse with a scalpel and forceps. The mouse was placed into a container with 500 ml of 10% neutral buffered formalin (Thermo Scientific, cat. no. 5725), at a 20:1 ratio of formalin to tissue. Whole body fixation required three days at room temperature prior to dissection. Following fixation, soft tissues (e.g. muscle, ligaments) were kept intact to assist with correct orientation of the bone specimen during the embedding process. An additional 24 hours were required for tissue decalcification with Surgipath Decal I Solution (Leica Microsystems, cat. no. 00440). Tissues were embedded in paraffin and processed for immunohistochemistry using Hematoxylin (Thermo Scientific, cat. no. 22-050-112) and Eosin-y (Fisher, cat. no. SE23-500D). Obtaining bone sections from the head of the femur to the patella was essential for

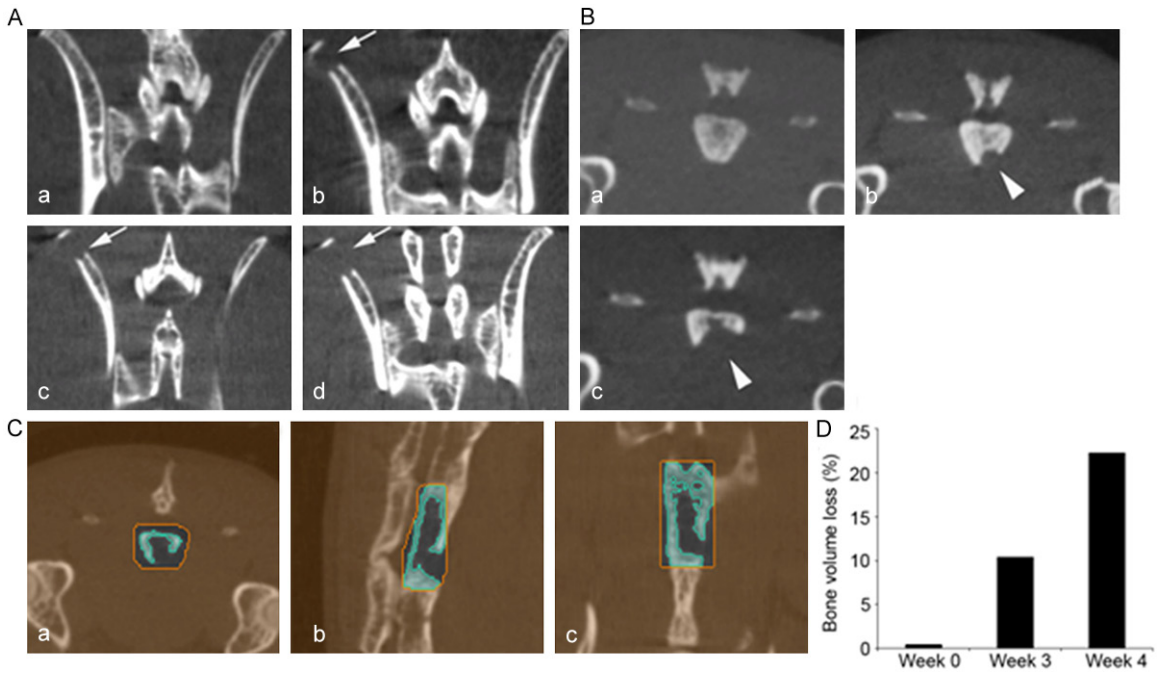

Figure 4. Intracardiac injection of PC3-B1 prostate cancer cells produced progressive axial skeletal lesions. (A) Micro CT images of lower vertebrae and hip region at 1 week (a) post tumor injection had detectable and progressive lesions in the iliac crest (arrows) at weeks 3 (b), 4 (c) and 5 (d) after tumor cell injection. (B) Micro CT images of mouse sacral vertebrae number 3 prior to injection (week 0, a) and weeks 3 (b), 4 (c) and 5 (d). Arrowheads demonstrate bone lesion progression. (C, D) Quantitative analysis of the sacral lesion (B) was performed using the axial (a), sagittal (b) and coronal (c) views of 3D images (C) using IRW software (Siemens). The sacral vertebrae 3 was selected in a ROI using all three views (orange) and segmentation was used (blue) to compute bone volume through all 3D slices in the ROI. The percent bone volume loss in the sacral vertebrae lesion is shown graphically (D) and demonstrates a 23% loss by 4 weeks.

matching to the micro CT image, with sections oriented such that the length of the femur was longitudinally sectioned into three micron slices. Consistent orientation and placement of the specimen into the block requires practice, skill and is a critical element in the procedure.

Matched micro CT and histopathology

Microscopy was used to ensure that each consecutive image overlapped the preceding image by a small amount (approximately 30 micrometers or 2-3 cell widths). Images were knitted together using Adobe Photoshop CS5 software. The sagittal CT images were viewed consecutively until a representative slice of the CT scan correlated with the knitted histology image (**Figure 3**). Accurate orientation of the bone in the block was critical for obtaining optimal longitudinal sections (**Figure 3**). Micro CT images were also rotated in three dimensions to match the histological sections.

Results

Intraosseous injection resulted in lytic lesion formation

Following intraosseous injection of PC3B1 cells, mice were evaluated each week, for 4 weeks using sequential micro CT imaging. Three dimensional reconstruction of the femur demonstrated that lesions first appeared near the head of the femur, consistent with placement of cells directly into the bone, approximately 0.3 cm proximal to the epiphyseal plate. By week 3, substantial erosion was observed at the epiphyseal region of the femur toward the patella (**Figure 1A**). Bone volume loss was quantified three weeks after the injection (**Figure 1B**), with distinct observable areas of eroded bone (**Figure 1A**, Inset b). All bone lesions resulting from intraosseous injection were lytic in nature and absent of new bone formation.

Intracardiac injection and the appearance of sclerotic lesions

Following intracardiac injection of PC3B1 cells, bone metastases in the femur and tibia were detected by week 3 and most frequently observed at the epiphyseal plate The intracardiac injection route is a clinically applicable model, given that bone metastases occur primarily in regions of active bone marrow in adults [16]. The majority of lesions produced via intracardiac injection were found to be progressive (**Figure 2**, Top); however, in a minority of cases, new endosteal bone formation was also observed in the intramedullary space, typical of a healing response (**Figure 2**, Bottom, white arrow) and observed in several animals by week 6 with apparent cessation of tumor progression by week 8. The intracardiac injection route was also found to produce lesions predominantly in the femur and tibial bones as early as three weeks (**Table 1**). Coinciding with other studies, lesions were also detected in the iliac crest and vertebral column [17]. In the vertebral column, matched histology revealed tumor in the bone marrow, resulting in replacement of the normal marrow elements with tumor in the affected section (**Figure 3B**).

Micro CT and matched histopathology of lesions

Micro CT is useful for chronologically tracking lesions to calculate lesion progression and for detection of lesions prior to imminent fracture. Bone histopathology provides important validation of tumor growth within the bone and can be used to provide valuable insights into mechanisms of tumor interaction within the bone microenvironment. **Figure 3** demonstrates the co-existence of two distinct lesions on the same bone; one lesion was observed to have breached the periosteum near the patella (arrow) and have osteolytic features; while the second lesion had sclerotic features and evidence of new endosteal bone formation (arrow).

Discussion

The ability to detect both vertebral and femoral lesions within the same xenograft model could vastly benefit future clinical studies. Other studies have shown that the presence of both axial and appendicular bone metastases result in worse outcomes compared to the presence of solely axial lesions [18]. Additionally, the intracardiac injection route produced lesions that mimic bone metastatic lesions known to occur in humans (e.g. sclerotic lesions). Clinically, sclerotic lesions observed in humans often signal a better prognosis and increased odds towards curative results following therapy [19], with approximately 50% of human prostate and breast tumors that arise in bone are described as sclerotic [20]. The current model allows for investigation into mechanisms of promoting or inhibiting sclerotic lesion growth, and could be exploited to determine histological and molecular features of lesions through matching histology with micro CT. Additionally, this model could be used to refine imaging technology, given that sclerotic lesions are often a source of false positives on human bone scans [19].

The spontaneous appearance of these differing lesions within the same bone, in genetically identical SCID mice that received the same cell line, suggests that this model may be useful for identifying indolent clones in the injected tumor population or discovery of systemic factors [5] to prevent cancer progression. This matched combination protocol could be utilized to facilitate discovery of new strategies inducing sclerotic bone lesions and limiting lytic lesions, investigation of new therapeutics preventing bone metastasis, and research strategies aimed at understanding mechanisms of tumor dormancy in bone.

Acknowledgements

This work was supported in part by NIH grants RO1 CA159406, P30 CA023074 and GM-008718. The work done by EMSS (Experimental Mouse Shared Service) and TACMASS (Tissue Acquisition and Cellular/Molecular Analysis Shared Service), supported by the University of Arizona Cancer Center Support Grant, NIH.

Disclosure of conflict of interest

None.

Address correspondence to: Dr. Anne E Cress, University of Arizona Cancer Center, University of Arizona, 1515 N. Campbell Avenue, Tucson, AZ 85724, USA. Tel: 520-626-7553; Fax: 520-626-4979; E-mail: cress@email.arizona.edu

References

[1] Mundy GR. Mechanisms of bone metastasis. Cancer 1997; 80: 1546-1556.

[2] Aguirre-Ghiso JA. Aguirre-Ghiso. Models, mechanisms and clinical evidence for cancer dormancy. Nat Rev Cancer 2007; 7: 834-846.
[3] Pantel K, Alix-Panabières C, Riethdorf S. Cancer micrometastases. Nat Rev Clin Oncol 2009; 6: 339-351.
[4] Arguello F, Baggs RB, Frantz CN. A murine model of experimental metastasis to bone and bone marrow. Cancer Res 1988; 48: 6876-6881.
[5] Gomes RR Jr, Buttke P, Paul EM, Sikes RA. Osteosclerotic prostate cancer metastasis to murine bone are enhanced with increased bone formation. Clin Exp Metastasis 2009; 26: 641-651.
[6] King T, Vardanyan A, Majuta L, Melemedjian O, Nagle R, Cress AE, Vanderah TW, Lai J, Porreca F. Morphine treatment accelerates sarcoma-induced bone pain, bone loss, and spontaneous fracture in a murine model of bone cancer. Pain 2007; 132: 154-168.
[7] Phadke PA, Mercer RR, Harms JF, Jia Y, Frost AR, Jewell JL, Bussard KM, Nelson S, Moore C, Kappes JC, Gay CV, Mastro AM, Welch DR. Kinetics of metastatic breast cancer cell trafficking in bone. Clin Cancer Res 2006; 12: 1431-1440.
[8] Ports MO, Nagle RB, Pond GD, Cress AE. Extracellular engagement of alpha6 integrin inhibited urokinase-type plasminogen activator-mediated cleavage and delayed human prostate bone metastasis. Cancer Res 2009; 69: 5007-5014.
[9] Christiansen JJ, Rajasekaran AK. Reassessing epithelial to mesenchymal transition as a prerequisite for carcinoma invasion and metastasis. Cancer Res 2006; 66: 8319-8326.
[10] King TE, Pawar SC, Majuta L, Sroka IC, Wynn D, Demetriou MC, Nagle RB, Porreca F, Cress AE. The role of alpha 6 integrin in prostate cancer migration and bone pain in a novel xenograft model. PLoS One 2008; 3: e3535.
[11] Rabbani SA, Valentino ML, Arakelian A, Ali S, Boschelli F. Boschelli. SKI-606 (Bosutinib) blocks prostate cancer invasion, growth, and metastasis in vitro and in vivo through regulation of genes involved in cancer growth and skeletal metastasis. Mol Cancer Ther 2010; 9: 1147-1157.
[12] Bouxsein ML, Boyd SK, Christiansen BA, Guldberg RE, Jepsen KJ, Müller R. Guidelines for assessment of bone microstructure in rodents using micro-computed tomography. J Bone Miner Res 2010; 25: 1468-1486.
[13] Sroka IC, Pond GD, Nagle RB, Porreca F, King T, Pestano G, Futscher BW, Gard JM, Riley J, Cress AE. Human Cell Surface Receptors as Molecular Imaging Candidates for Metastatic Prostate Cancer. Open Prost Cancer J 2009; 2: 59-66.
[14] van Bokhoven A, Varella-Garcia M, Korch C, Hessels D, Miller GJ. Widely used prostate carcinoma cell lines share common origins. Prostate 2001; 47: 36-51.
[15] Johnson LC, Johnson RW, Munoz SA, Mundy GR, Peterson TE, Sterling JA. Longitudinal live animal micro-CT allows for quantitative analysis of tumor-induced bone destruction, Bone 2011; 48: 141-151.
[16] Jacobs SC. Spread of prostatic cancer to bone. Urology 1983; 21: 337-344.
[17] Burch S, Bisland SK, Wilson BC, Whyne C, Yee AJ. Multimodality imaging for vertebral metastases in a rat osteolytic mode. Clin Orthop Relat Res 2007; 454: 230-236.
[18] Wyatt RB, Sánchez-Ortiz RF, Wood CG, Ramirez E, Logothetis C, Pettaway CA. Prognostic factors for survival among Caucasian, African-American and Hispanic men with androgen-independent prostate cancer. J Natl Med Assoc 2004; 96: 1587-1593.
[19] Scher HI, Morris MJ, Basch E, Heller G. End points and outcomes in castration-resistant prostate cancer: from clinical trials to clinical practice. J Clin Oncol 2011; 29: 3695-3704.
[20] Conti G, La Torre G, Cicalese V, Micheletti G, Ludovico MG, Vestita GD, Cottonaro G, Introini C, Cecchi M. Prostate cancer metastases to bone: observational study for the evaluation of clinical presentation, course and treatment patterns. Presentation of the METAURO protocol and of patient baseline features. Arch Ital Urol Androl 2008; 80: 59-64.